PLASTIC SCINTILLATOR TARGET TRACKER PROPOSAL (BASELINE) AND STUDIES DONE AT STRASBOURG

R. Arnold, E. Baussan, <u>M. Dracos</u>, J–L. Guyonnet
J. Cailleret, E. Gamelin, G. Gaudiot, B. Humbert,
R. Igersheim, T–D. Le, D. Staub, D. Thomas, J. Wurtz

IReS, IN2P3–CNRS/Université Louis Pasteur
BP 28, F-67037 Strasbourg Cedex 2, France.

Abstract

In this document we present the plastic scintillator target tracker baseline option as it is already defined in the OPERA proposal. Details are given according to the internal referees requests. Various test on WLS fibres, plastic scintillators and photomultipliers are summarised. The full scale plastic scintillator prototype construction and measurements done with this prototype are also presented.

1. Introduction

The baseline option for the electronic detectors placed in the target section of the OPERA detector are scintillator strips, 6.7 m length, 1 cm thick, 2.6 cm wide, read using Wave Length Shifting (WLS) fibres and photodetectors placed at both ends of the fibers [1]. The scintillator strips are supposed to be obtained by extrusion, with a TiO_2 co-extruded reflective coating for better light collection. A 6.7 m long groove, 2.0 mm deep, in the centre of the scintillator strip houses the WLS fibre which is glued in the groove.

The Hamamatsu 64–channel photomultiplier tube (PMT) H7546 [2] has also been chosen as baseline photodetector to read the WLS fibres.

In this document we support the baseline option to become the final choice for the OPERA target tracker.

2. Geometry

A basic unit of the baseline target tracker is constituted by 64 strips readout by WLS fibres coupled to a single 64–pixel photodetector. Four such modules will be assembled in situ to construct a whole scintillator plane in order to cover the 6.7×6.7 m^2 sensitive surface defined by the target bricks. One plane of 4 modules of parallel strips and one plane of 4 modules of vertical ones form a scintillator wall providing an $x - y$ track information (Fig. 1). This assembly system has the advantage to allow the parallel production of detectors
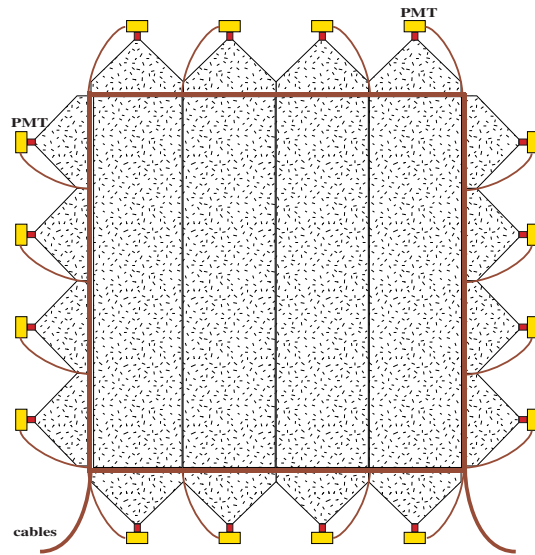

Figure 1. Schematic view of a plastic scintillator strip wall as defined in the OPERA proposal.

in several sites and minimize the mounting time in the underground Gran Sasso laboratory. The quantities of the various detector components are reported in Table 1.

In the proposal we have proposed to subdivide the modules in 4 groups of 16 strips each enclosed in a light-tight aluminium case 0.5 mm thick to provide the needed
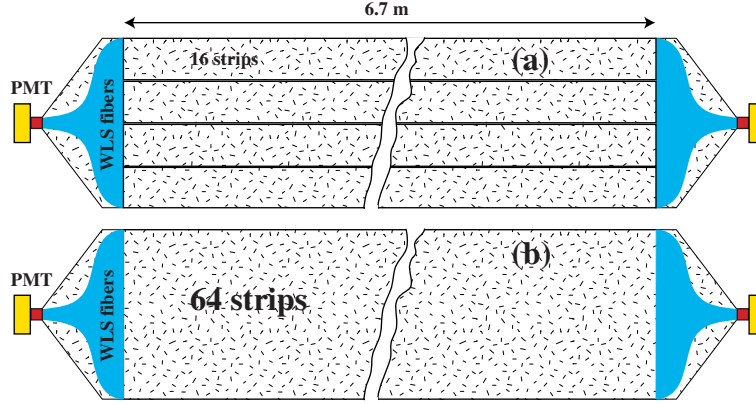
Figure 2. Schematic view of a scintillator strip module as defined in the OPERA proposal (a) and new proposal (b).

Table 1. Summary of the main numbers for the target electronic trackers.

Number of detector components	per plane	per wall	for the full detector
Scintillator modules	4	8	576
Scintillator planes	1	2	144
Scintillator strips	256	512	36864
PMT's	8	16	1152

mechanical strength. The construction of the prototype has proven that this subdivision is not necessary. Indeed, by gluing the 64 strips of the module together, the mechanical strength is given by the strips themselves and not any more by the aluminium cases. Thus, the dead space produced by the aluminium sheets is reduced from 2.5 mm to 1 mm per module (Fig. 2). Moreover, the construction becomes easier and the accident risks (breaking fibres or strips) are considerably reduced.

The fibres are directly routed at both ends to the photodetectors through the end–manifolds (Fig. 3). The total end–manifold length is imposed by the minimum fibre bending radius which is of the order of 6 cm, the photodetector and cookie length (about 7 cm), the electronic readout card (5 cm) and a rigid part less than 10 cm length necessary to support the other modules in the same plane. Thus, the total length does not exceed 40 cm, length imposed by the the brick manipulator robot group.

The end–manifold has a thickness of 11 mm near the scintillator strips and 32 mm at the level of the photodetector imposed by the Hamamatsu multianode PMT thickness (30 mm leaving 1 mm margin on each side). The high voltage and readout cables can be extracted and routed through a narrow column near the scintillator strips (Fig. 3).

For the wall handling two options are proposed. In the first one (called option 1), shown schematically by Fig. 4, the scintillator walls are suspended on I–beams independently of the brick walls. The vertical modules are directly suspended on the I–beams while the horizontal modules are suspended on one another. In the second option (option 2) the horizontal modules are suspended on the brick walls (Fig. 5). The advantage of option 1 is that the target tracker construction is independent of the brick wall construction and any brick wall displacement during brick mounting. But, in this case the end–manifolds of the horizontal modules must be rigid enough to support the other modules while for option 2 this is not necessary reducing thus the end–manifold length by about 10 cm. Module deformations (very probable over 6.7 m) will not be a problem for option 1 while for option 2 this point is more critical. In option 2, the fixing system on brick walls must be strong enough to support the modules weight (275 Kg each).

For option 1 the total minimum wall thickness in sensitive area is 24 mm (strip thickness=10 mm, aluminium sheets=1 mm, glue+TiO_2=1 mm per plane). At least 1 mm tolerance must be added on each side of a plane increasing the total wall thickness to about 28 mm. For option 2 the total wall thickness is the one of option 1 plus 2 mm for the fixing of the horizontal planes on the brick walls giving a total thickness of 30 mm. One can see that the minimum distance between two brick walls (important for "brick reconnection" and emulsion scanning load), in case the photodetectors are
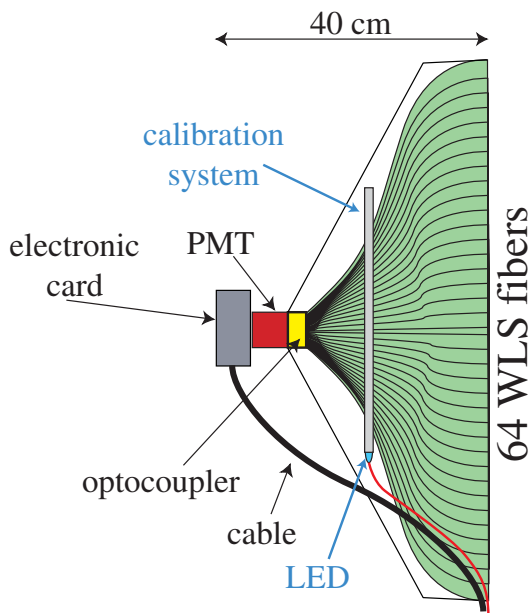
Figure 3. End–manifold of the scintillator strips module.

Figure 5. Wall handling for option 2.

not placed in front of the modules but on the corners of each wall, is of the order of 28 mm, i.e., a marginal reduction of only 4 mm compared to the case where the
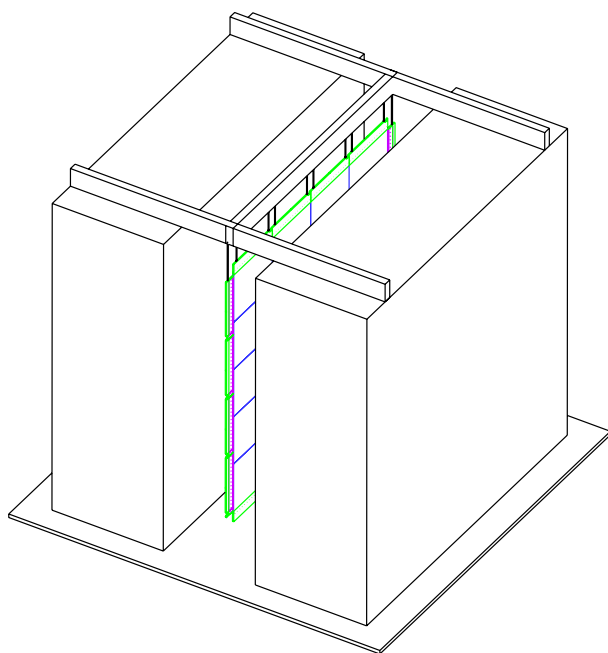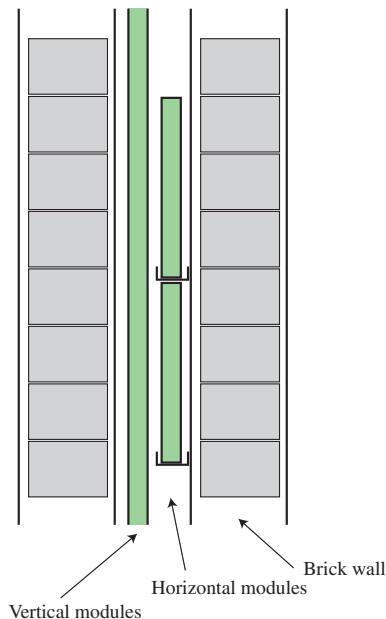
photodetectors are in front of the modules. But, in the case where the photodetectors are placed on the plane corners, handling, mounting and optical connection problems with clear fibres have to be solved. Indeed, in this case the end–manifolds have to be mounted on the modules in situ and connect carefully clear fibres on WLS fibres. This delicate operations would have to be done first of all in the construction institutes in order to calibrate the modules and must be hopefully reproduced during the mounting operation in the tunnel. Option 1 has been chosen for the prototype construction.

Finally, the dead space induced by the aluminium module envelop and the scintillator strip TiO_2 wrapping (0.15 mm thick) is of the order of 1.2% of the overall sensitive surface.

3. Plastic scintillators and WLS fibres

The quality of plastic scintillators and WLS optical fibres is very important for a high track detection efficiency.

3.1. WLS fibres

A very important parameter of WLS fibres is their attenuation length. Several double clad fibres which are commercially available from Bicron‡, Kuraray§ and

Figure 4. Wall handling for option 1.

‡ Bicron Corp., 12345 Kinsman Road, Newbury, Ohio 44065.

§ Kuraray Co., Methacrylic Resin Division, 8F, Maruzen Building, 3-10, 2-Chrome, Hihonbashi, Chuo-ku, Tokyo, 103-0027, Japan.
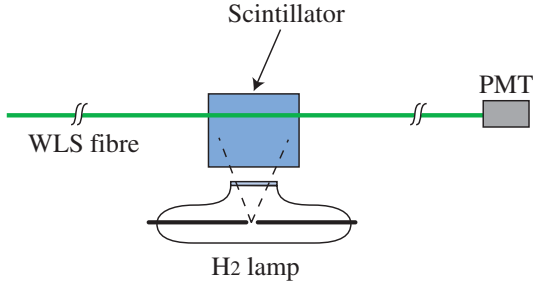
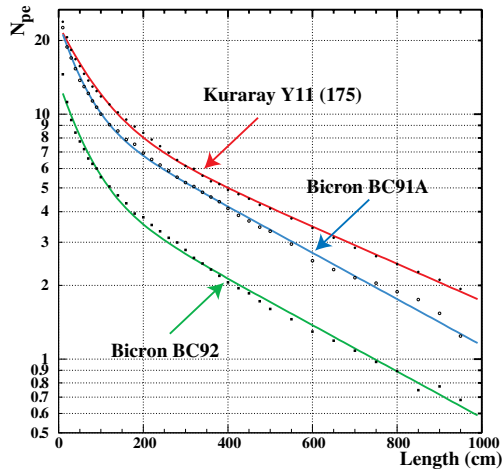**Figure 6.** Setup for WLS fibre attenuation study.

Table 2. Fitted parameters of the WLS fibres. The fitted distribution was: $e^{a_s - x/\lambda_s} + e^{a_l - x/\lambda_l}$ (units in cm).

Fibre type	a_s	λ_s	a_l	λ_l
Kur. Y11 (175)	2.59	79.0	2.29	573.2
BC91A	2.62	52.2	2.30	460.0
BC92	2.14	58.2	1.62	460.1

Figure 8. Comparison between Kuraray fibres.

Figure 7. Fibre attenuation study using Kuraray and Bicron fibres.

Pol.Hi.Tech‖ have been tested.

The setup used to measure the attenuation in the fibres versus the distance is shown by Fig. 6. A H_2 U.V. lamp has been used to excite a NE110¶ scintillator. The light emitted by the scintillator is collected by the WLS fibre. Thus, the light spectrum seen by the WLS fibre is the one in real experiment. The distance between the PMT (Hamamatsu bialkali R1635) and the illumination point is variable (up to 10 m).

Fig. 7 shows the collected light intensity versus the distance for 3 different WLS fibres all of them having a diameter of 1 mm. The equivalent number of p.e given in $y - axis$ is obtained by normalization after a measurement done with a scintillator strip and BC91A fibre as described in the subsection 3.2 and it is given
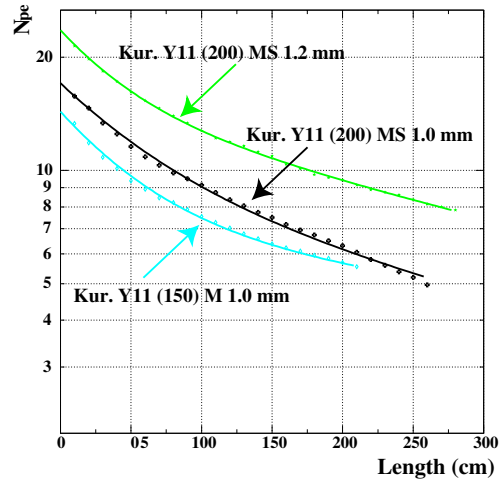
‖ Pol.Hi.Tech. s.r.l., 67061 CARSOLI (AQ), S.P. Turanense Km. 44.400, Italy.

¶ Nuclear Enterprise.

just for indication. The fitted curves are the sum of 2 exponential distributions: $e^{a_s - x/\lambda_s} + e^{a_l - x/\lambda_l}$ (units in cm). The fitted values of the parameters are given in table 2. As one can see, the Kuraray Y11 (175) WLS fibre gives the best results. The two Bicron fibres have the same absorption lengths but the light yield is significantly different.

Fig. 8 shows a comparison between several Kuraray fibres, while Fig. 9 compares two Kuraray fibres of 1.0 mm and 1.2 mm diameter. The ratio of these last two measurements is given by Fig. 10 and depends on the distance. At a 0 distance this ratio is about 1.4 and goes down to 1.1 at 6 m. Fig. 11 and 12 show the same comparison but for Pol.Hi.Tech fibres. Finally, Kuraray Y11 (175) fibres are considered been the best for our application.

3.2. Scintillators

Several plastic scintillators produced by different companies have been tested at Strasbourg using the setup shown by Fig. 13. The tests have been done by irradiating the scintillator strips by electrons of 1.8 MeV selected from a ^{90}Sr β source with the help of a well
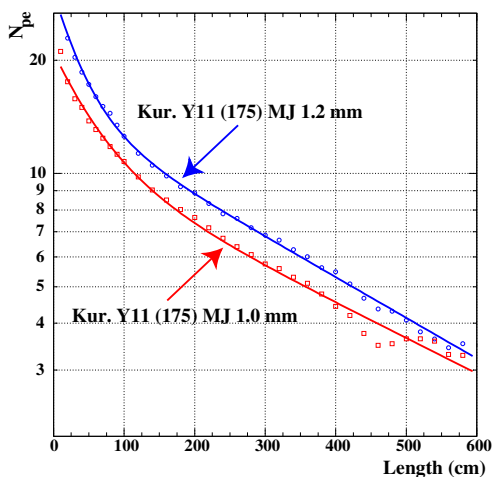
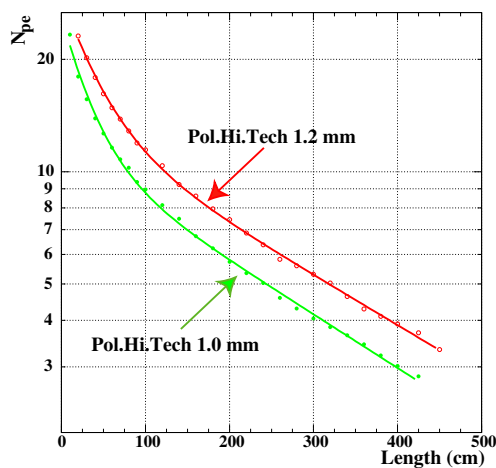**Figure 9.** Comparison between two Kuraray fibres of 1.0 mm and 1.2 mm diameter.

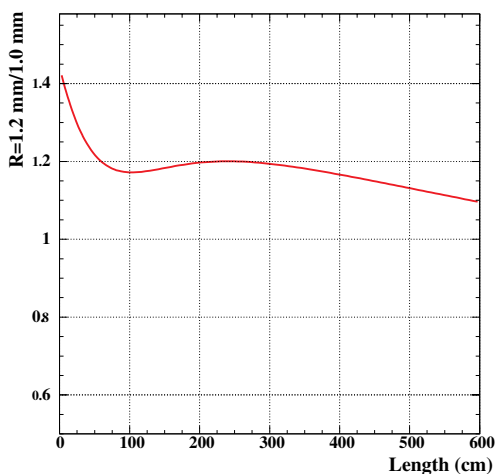**Figure 11.** Comparison between two Pol.Hi.Tech fibres of 1.0 mm and 1.2 mm diameter.

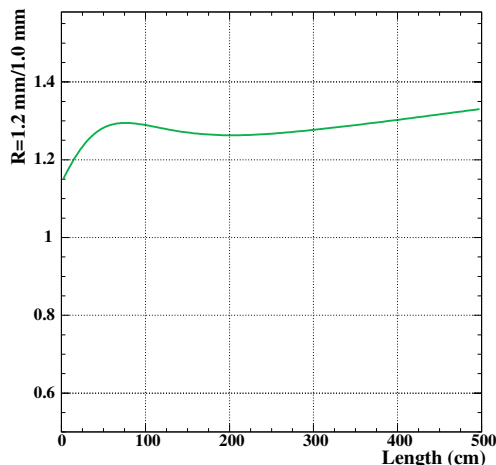**Figure 10.** Ratio of the two measurements of Fig. 9.

Figure 12. Ratio of the two measurements of Fig. 11.

calibrated magnetic spectrometer (Fig. 14). An electron trigger at the exit of the spectrometer is provided by a 100 μm thick scintillator slide which is read on its two opposite sides by two PMT's in coincidence. The signal readout was done by two Hamamatsu bialkali PMT's R6091 through a WLS fibre glued in a groove, 1.6 mm depth, performed at the scintillator surface.

Table 3 gives the mean light in ADC counts collected by each PMT. The result obtained by a strip with the same geometry made by NE110 scintillator material is also given. This last sample providing

10.5 photoelectrons (p.e) at each side is considered as acceptable for OPERA and NE110 quality will be used as reference. From these results we estimate that, for our application, the two first extruded samples (AMCRYS-H^{+} UPS-98M, UPS-96M) are not appropriate while the other three are very good. Very promising is the result obtained from the Pol.Hi.Tech sample extracted from a 4 m extruded scintillator strip produced for I216 proposed experiment [4].

[+] AMCRYS-H, 60, Lenin ave, Kharkov, 310001, Ukraine.

Table 3. Scintillator comparison. The given light intensity (underlined numbers) comes from our measurements while all other information has been given by the producer.

|	
Scintillator: AMCRYS-H UPS-98M	Light in ADC counts = 459
Production method	Extrusion
Base material	Specially purified and polymerized polystyrene
Scintillation additives	PTP (2%), POPOP (0.02%)
Light yield, % to anthracene	50
Bulk attenuation length, cm	40
Sample width, cm	2.0
Scintillator: AMCRYS-H UPS-96M	Light in ADC counts = 506
Production method	Extrusion
Base material	Standard polystyrene (BASF)
Scintillation additives	PTP (2%), POPOP (0.02%)
Light yield, % to anthracene	50
Bulk attenuation length, cm	20
Sample width, cm	2.0
Scintillator: AMCRYS-H UPS-89	Light in ADC counts = 1208
Production method	Bulk polymerization
	Mechanical cutting and polishing
Base material	Specially purified and polymerized polystyrene
Scintillation additives	PTP (2%), POPOP (0.02%)
Light yield, % to anthracene	50
Bulk attenuation length, cm	100-150
Sample width, cm	2.0
Scintillator: AMCRYS-H UPS-90	Light in ADC counts = 1142
Production method	Bulk polymerization
	Mechanical cutting and polishing
Base material	Specially purified and polymerized polystyrene
Scintillation additives	PTP (2%), POPOP (0.02%)
Light yield, % to anthracene	50
Bulk attenuation length, cm	150-200
Sample width, cm	2.0
Scintillator: AMCRYS-H UPS-923A	Light in ADC counts = 1368
Production method	Bulk polymerization according to special regime of polymerization
	Mechanical cutting and polishing
Base material	Specially purified and polymerized polystyrene
Scintillation additives	PTP (2%), POPOP (0.02%)
Light yield, % to anthracene	50
Bulk attenuation length, cm	250-300
Sample width, cm	2.0
Scintillator: Pol.Hi.Tech	see tests in the following sections
Production method	Extrusion in normal atmosphere
Base material	Polymerized polystyrene
Scintillation additives	PPO (1%), POPOP (0.03%)
Sample width, cm	2.0
Scintillator: Kuraray (MINOS)	Light in ADC counts = 623
Production method	Extrusion for MINOS
Base material	Polymerized polystyrene
Sample width, cm	4.0
Scintillator: NE110	Light in ADC counts = 1114
Production method	Mechanical cutting and polishing
Density	1.032
Decay time, ns	3.3
Sample width, cm	2.0
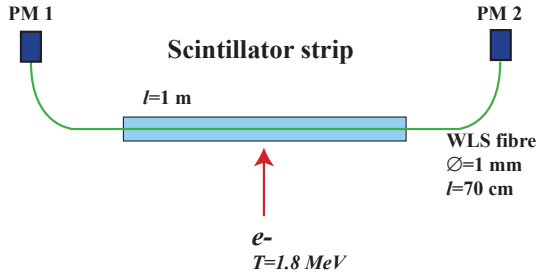
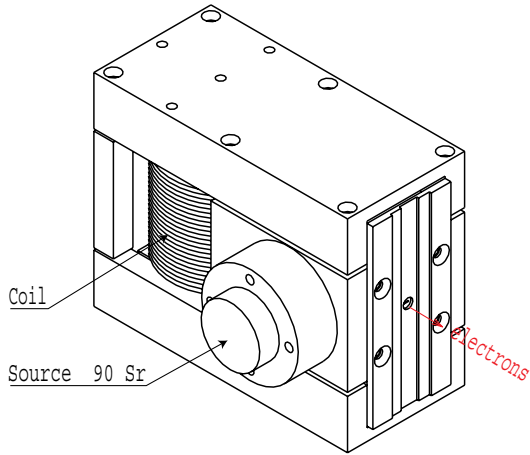**Figure 13.** Setup used for scintillator comparison using an electron spectrometer.

Figure 14. Electron spectrometer.

3.3. Test of scintillator strips and glued WLS fibres

To extract the number of p.e from full length scintillator strips equipped with WLS fibres and estimate the track detection efficiency at any place of the detector, the electron spectrometer has been used.

Fig. 15 presents the number of p.e, obtained by using a similar setup than the one of Fig. 13, versus the spectrometer electron kinetic energy. A very good linearity is observed.

Two scintillator Pol.Hi.Tech samples extruded for I216 proposed experiment and machined to have the OPERA geometry (2.6×1.0 cm^2) have been compared. The first one called "milky" due to its white aspect has been extruded in uncontrolled humidity atmosphere contrarily to the second sample. Surprisingly, the "milky" sample was presenting about 18% more light than the second one. This was probably due to a better diffusion of the light on diffusion centres produced by humidity. Fig. 16 presents the comparison of the two samples.

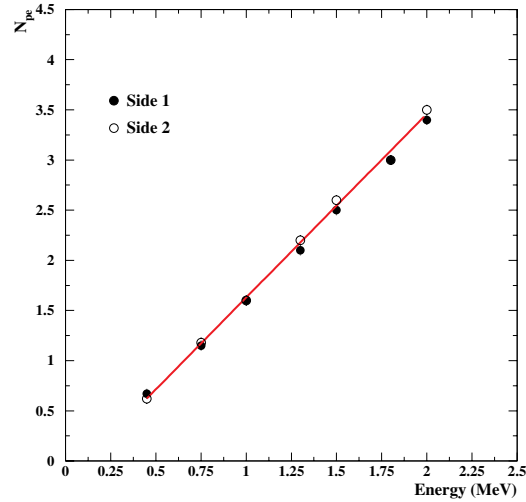Before the photons are collected by the WLS fibre

Figure 15. Number of detected photoelectrons versus the spectrometer electron energy.
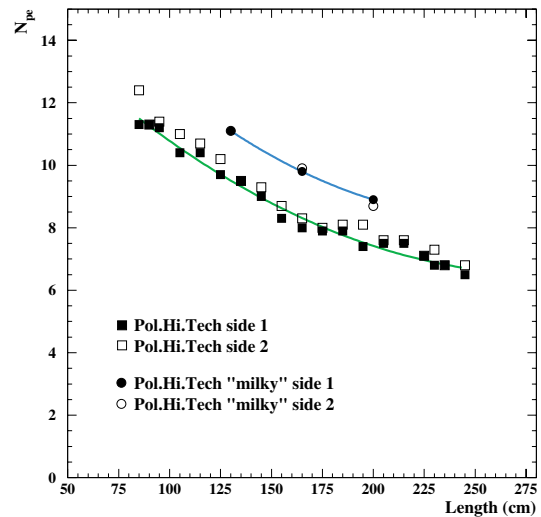

Figure 16. Number of p.e versus distance for Pol.Hi.Tech scintillator samples.

they make more than 10 reflexions on the strip surface and can be detected far away from the production point. To study the spatial expansion of the photon detection position by the WLS fibre, the setup shown schematically by Fig. 17 has been used. In a scintillator strip, a 3 cm WLS fibre has been glued between two clear fibres glued at both ends of the WLS fibre. Using the spectrometer (1.8 MeV electrons), the scintillator strip has been irradiated at several positions w.r.t. the WLS fibre position. Fig. 18 presents the amount of light collected at both clear fibre ends. A gaussian
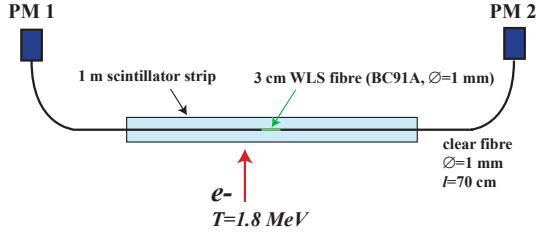
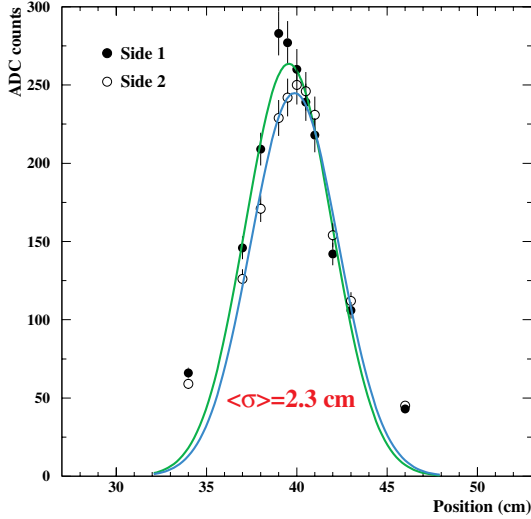**Figure 17.** Schematic view of the setup used for light collection study.

Figure 18. Light collection versus the position of the WLS fibre piece.

Figure 19. Light collection versus radiation position in a 1 cm thick and 4 cm wide scintillator strip.
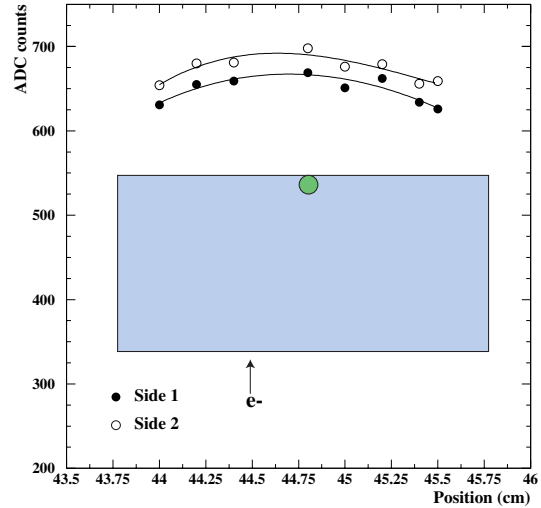
Figure 20. Light collection versus radiation position in a 1 cm thick and 2 cm wide scintillator strip.

distribution has been fitted on the data with an r.m.s. of 2.3 cm.

To study the light collection across a scintillator strip width and mainly near the strip edges and the fibre position, strips has been scanned with the electron spectrometer. Fig. 19 presents the measurement using a 4 cm wide strip while Fig. 20 and 21 show the results using a 2.0 cm and 2.6 cm wide Pol.Hi.Tech strips. Near the edge of the strip a loss of light is observed due to escaping electrons as shown by the GEANT simulation of Fig. 22. This, of course, will not happen for minimum ionizing particles.

Electrons with an energy around 1.8 MeV can mimic the energy loss of minimum ionizing particles (MIP). Tests with a pion beam at PS (CERN) have been done in order to verify the above assumption. Nevertheless, the ratio between the measurements done with the PS beam and those done with the electron spectrometer has been found to be 1.15. This deviation from unity is due to the contribution of backscattered
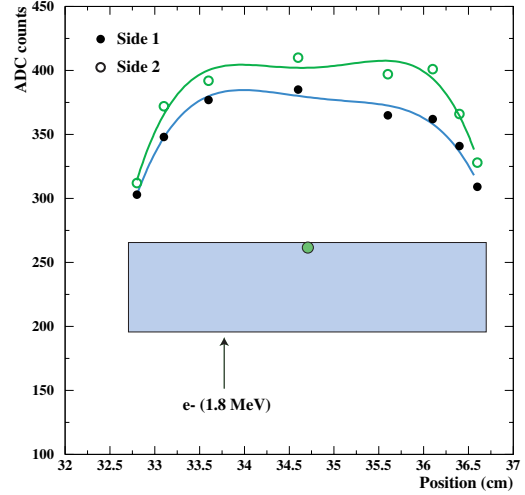
and out of energy electrons in the case of using the spectrometer (more details are given in section 6). Fig. 23 presents the light collection in both ends of a 2 m scintillator strip equipped with a BC91A 1.0 mm fibre versus the beam angle. A very clear $\cos\theta_{beam}$ dependence as expected is observed.

Fig. 24 presents a comparison between a bialkali and a multialkali photocathode using the scintillator test setup. For this comparison, the two Hamamatsu PMT's H3164–10 (bialkali) and R7400U-02 (multialkali) have been used. With a multialkali photocathode a factor of 1.6 more light is collected compared to the bialkali
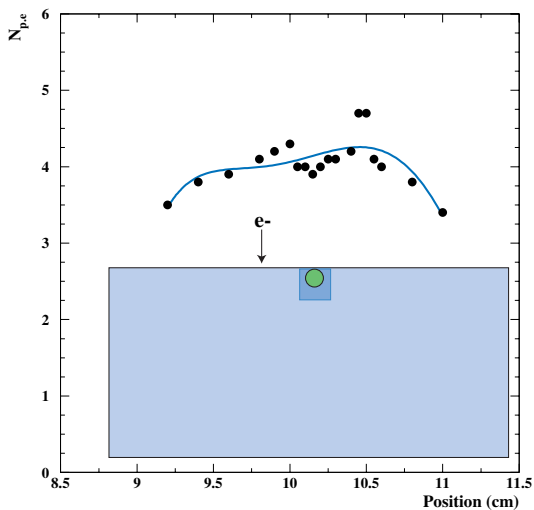
Figure 21. Number of p.e versus radiation position in 2.6 cm wide prototype scintillator strip at a distance of 330 cm from the PMT.
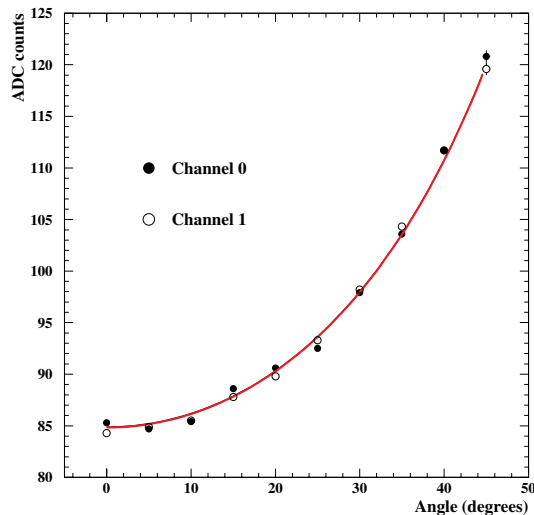

Figure 23. Light (in ADC counts) versus the beam angle w.r.t. the normal incidence on the scintillator strip (the fitted curve is proportional to $\cos\theta_{beam}$).
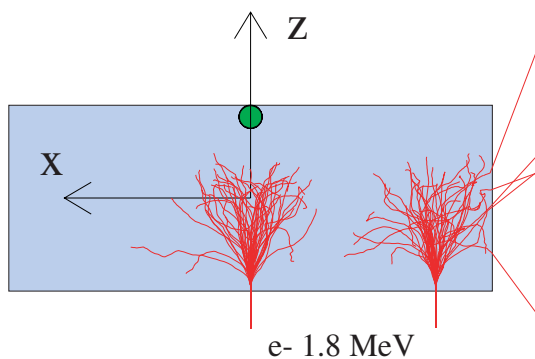

Figure 22. GEANT simulation of 50 1.8 MeV electrons entering in a 1 cm thick and 2.6 cm wide scintillator strip at two different positons in x.

gain uniformity among channels, linearity and cross talk. The baseline photodetector for the OPERA Target Tracker is the commercially available 64-channel Hamamatsu H7546 PMT (Fig. 26 and 27). This PMT has also been chosen for the MINOS [3] near detector and has been extensively evaluated. The characteristics of this PMT provided by Hamamatsu are given in Table 4.
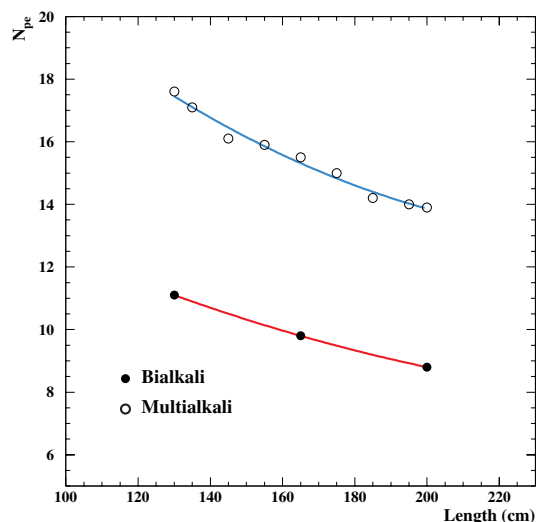
one. This number doesn't seem to depend on the distance (over 2 m) and can be explained by the different Quantum Efficiency spectra (Fig. 25).

An academic comparison has also been done between a 2.6×1 cm^2 (OPERA geometry) and 1×1 cm^2 (liquid scintillator geometry) cross section strips. This ratio has been measured using the electron spectrometer and the PS beam and found to be between 1.5 and 1.9.

4. Photodetector

The choice of the photodetector is mainly based on the single photoelectron detection efficiency, the dynamic range and the cost. Other considerations are

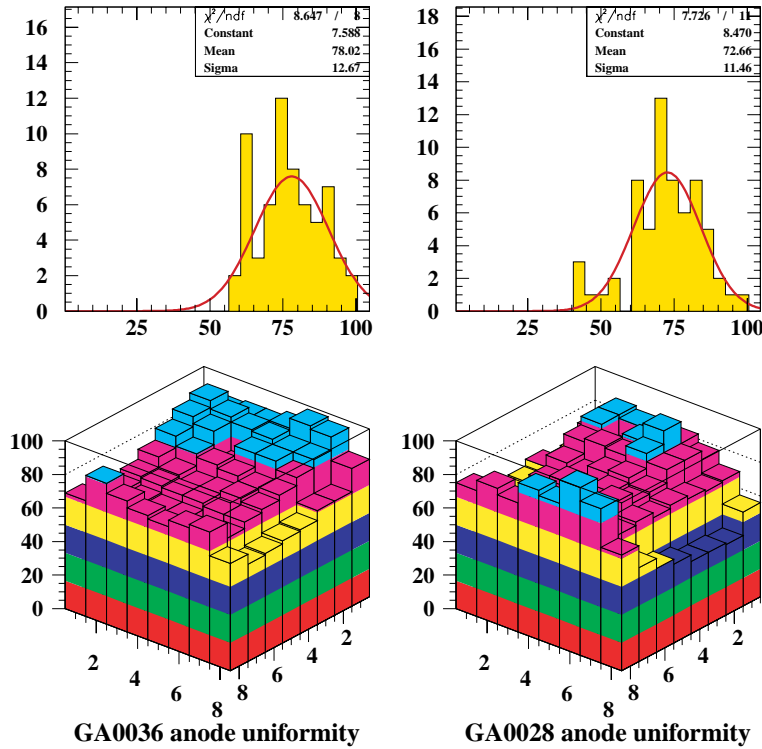**Figure 24.** Comparison between bialkali and multialkali photocathode.

Figure 28. Response of two 64–channels Hamamatsu H7546 PMT's, GA0036 and GA0028, at 800 V. The signal values are normalised to 100.

Each channel is constituted by two sets of 12 dynodes and each cell covers a surface of $2.3 \times 2.3 \, \text{mm}^2$. The PMT provides an output of the last dynode number 12. This signal common to all channels could be used as a FAST-OR to trigger the acquisition system or for timing purposes.

Advanced tests of the PMT's have been performed. Fig. 28 presents the channel response (normalised to 100) for an anode-cathode voltage of 800 V for the tubes under test obtained by full photocathode illumination using a W–lamp [2].

A more elaborated test system has been prepared to study in details the M64 PMT performance. This is schematically shown in Fig. 29. A computer guided translation system and the PMT are enclosed in a light-tight box together with a H_2 lamp, a band–pass filter and focalisation optics. With this system, a fine light spot ($< 50 \, \mu m$) can be produced at any place of the PMT photocathode allowing the scanning of the whole sensitive surface. By removing the focalisation lens near the PMT, the light beam can uniformly illuminate the whole photocathode. This option can be used for massive production tests. The PMT, to be in real conditions, can also be illuminated through a WLS fibre as shown by Fig. 30. The H_2 U.V. lamp excites a piece of scintillator in which the WLS fibre is glued.

Fig. 31 presents the PMT gain after a fine scan around channel 10 while Fig. 32 presents schematically the scanning points and the approximate position of the two dynodes of the channel. This scan has been done using a 1.0 mm fibre and reduced light intensity (single p.e level) in order to study the p.e collection and gain variations over one cell. Fig. 33 shows the charge distribution at one scanning point. A gaussian distribution convoluted with a poissonian one has been fitted for the signal. A gaussian distribution has also been used for the pedestal. The number of p.e collected at each position is presented by Fig. 34 while Fig. 35 gives the same number over a line passing by the middle of the two dynodes. A loss of p.e collection of the order of 6% is observed when the fibre is positioned between the two dynodes as it will be in the experiment. Fig. 36 presents the gain at 850 V observed on all channels when the fibre is in front of each dynode of the same channel and at the middle of the two. The maximum dispersion between the two dynodes of the same channel is of the order of 20%. On the same figure the gain resolution is also given.

The counting rate induced by natural radioactivity or PMT dark current must be as low as possible to

Table 4. Characteristics of the 64-channel Hamamatsu H7546 PMT.

Photocathode material	bialkali
Window material	borosilicate
Spectral response	300-650 nm
Wavelength of maximum response	420 nm
Number of dynode stages	12
Anode size	2×2 mm^2
Maximum supply voltage between anode and cathode	1000 V
Divider circuit	$3 : 2 : 2 : 1 : \cdots : 1 : 2 : 5$
Divider current at 1 kV	455 μA
Gain at 800 V	3.0×10^5
Cross talk (with 1 mm optical fibre)	2%
Uniformity among all anodes	1:3
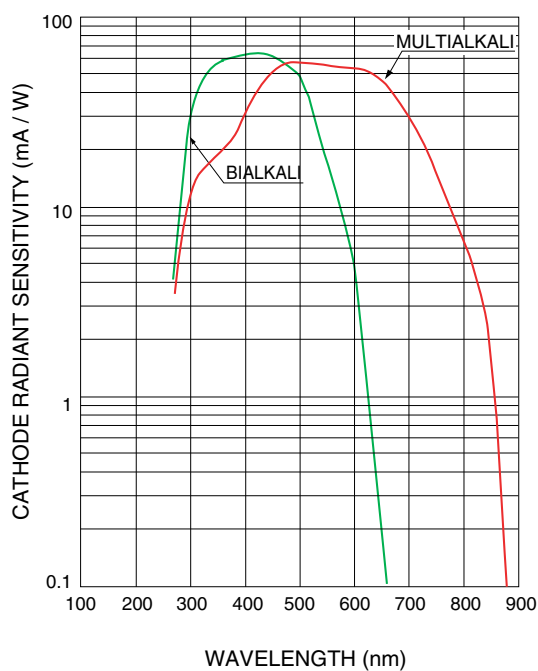
Figure 25. Comparison between bialkali and multialkali cathode radiant sensitivity [2].
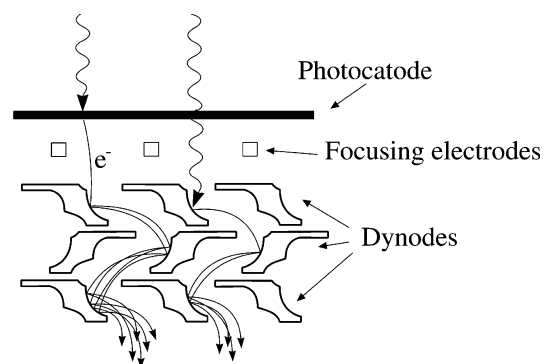
Figure 26. Multiplication process in a multianode PMT.
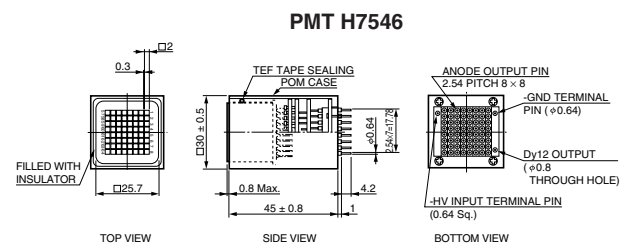
Figure 27. The 64-channel Hamamatsu H7546 PMT.

reduce the effect of dead time. Using the Hamamatsu 64–channel PMT with a threshold corresponding to $1/3$ photoelectron (p.e), a noise less than 10 Hz has been measured coming from photocathode thermoemission. This possibility of using a low threshold assures a very high single p.e detection efficiency and attenuates considerably the effect of the gain dispersion between PMT channels.

5. Monitoring and calibration systems

A monitoring and calibration system will be necessary to respectively test and calibrate the detector.

All data can be recorded in the same format than normal data. These data can be analysed off–line by the calibration and monitoring algorithms.
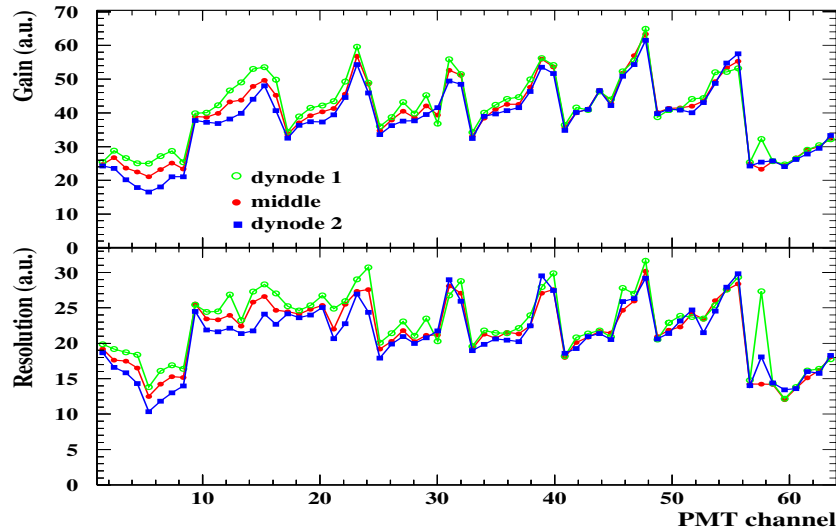
Figure 36. Gain and resolution of each PMT channel when the fibre is at the middle of the channel and in front of each dynode.
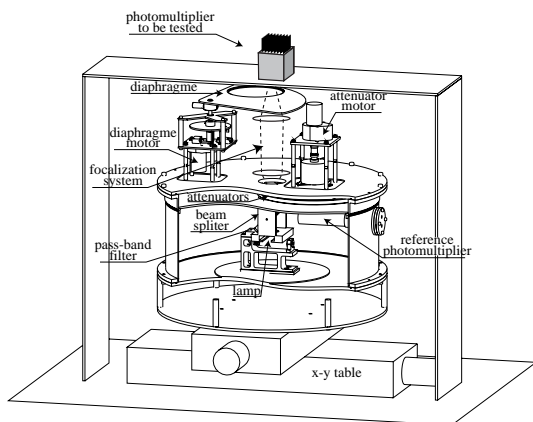

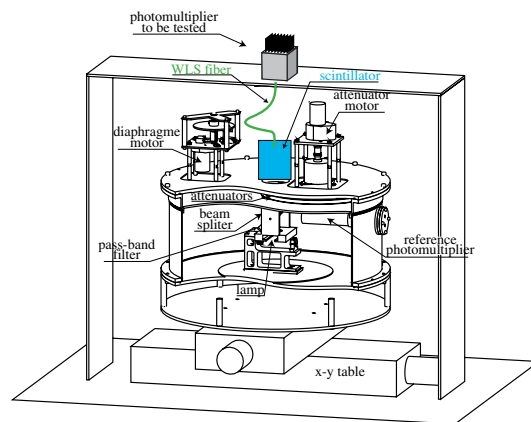**Figure 29.** Schematic structure of the PMT test system using a H_2 lamp.

Figure 30. Schematic structure of the PMT test system using a WLS fibre.

5.1. Monitoring system

The role of the monitoring system will be to test all the electronic channels and acquisition system. Fig. 3 shows schematically a light injection system for monitoring purposes. Light is injected in the WLS fibres at the level of the end–manifolds with the help of a LED and a PMMA (Polymethyl Methacrylate) strip. The LED is pulsed from outside and thus, an external trigger is also provided to the system. With this system all the PMT channels, the electronics and the acquisition system are tested in a very short time. By pulsing the LED on one side of the module and reading the signal on the other side, the WLS fibre ageing (if any) can also be monitored. A gain calibration at the level of single p.e can also be performed.

This system will be particularly helpful for detector and DAQ debugging during the detector installation.

5.2. Calibration system

All the scintillator modules will be calibrated using radioactive sources or an electron spectrometer in the construction institutes. In–situ, only the time evolution of the scintillator strips has to be followed and compared to the initial point.

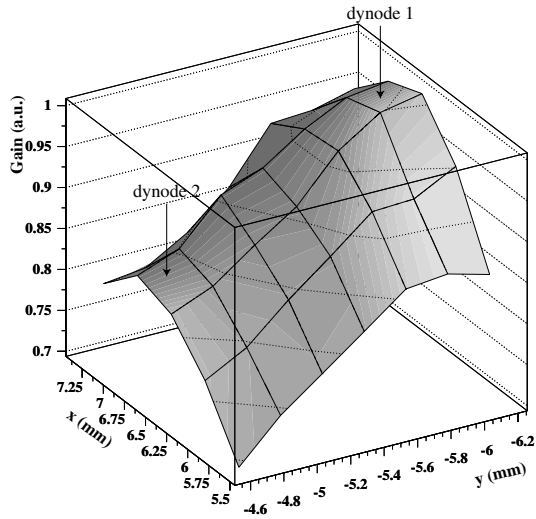Irradiating the scintillator strips using a radioactive source after they have been mounted in the detector

Figure 31. Gain variation over one cell as indicated by Fig. 32.

Figure 33. Charge distribution recorded at one scanning point.

construction, a piece of 46.5 mm is cut (taken into account during the strip production). 144 optically isolated pieces glued together form a strip of the same length than the normal scintillator strips. The 36864 pieces can be mounted in 4 extra scintillator modules as the one shown in Fig. 2.

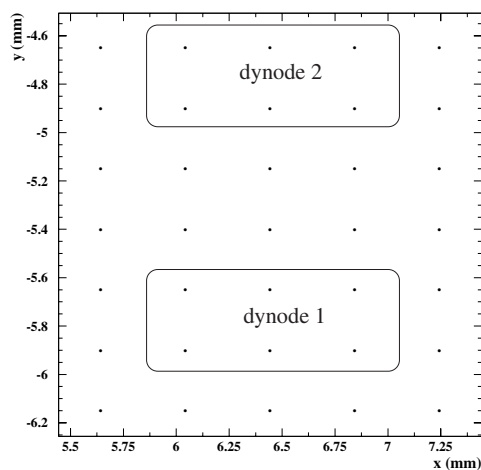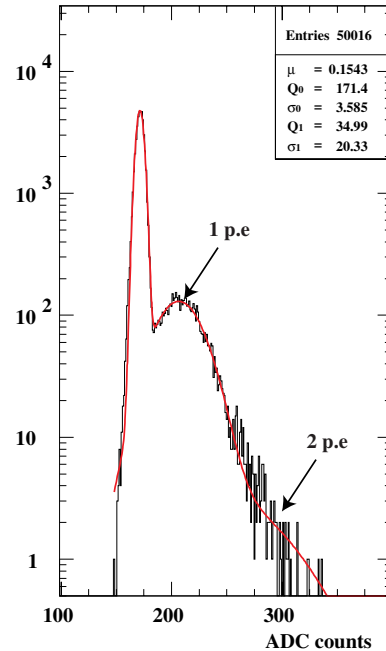The 4 modules can form an extra scintillator plane

Figure 32. Scanning points over one PMT cell. The approximate positions of the two dynodes are also shown.

necessitates extra mechanical systems and, more difficult, space and complicated operations. An extra difficulty comes from the fact that the emulsion bricks in the vicinity must not be irradiated. Use of cosmic rays, rock muons or natural radioactivity is prohibited due to the expected low statistics and complicated charge distributions and normalizations.

A simple and cheap system to follow the scintillator strips and glue (used for fibre gluing) ageing is what we will call in the following the "Domino Calibration System" (DCS): From each scintillator strip, during
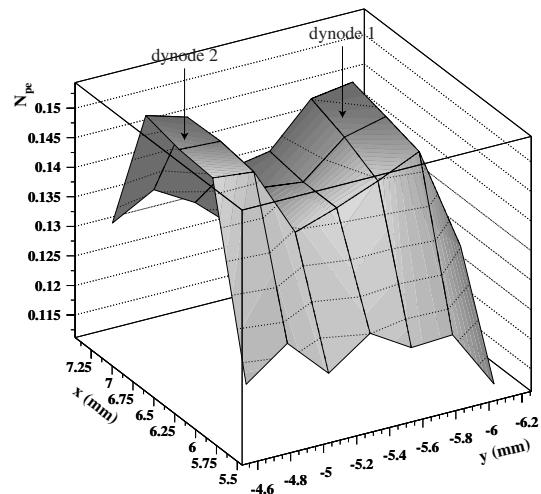

Figure 34. Number of p.e variation over one cell as indicated by Fig. 32.
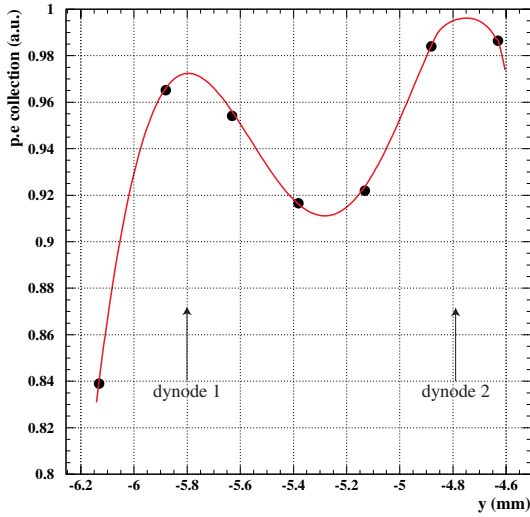
Figure 35. Number of p.e variation on a line passing by the middle of the two dynodes.
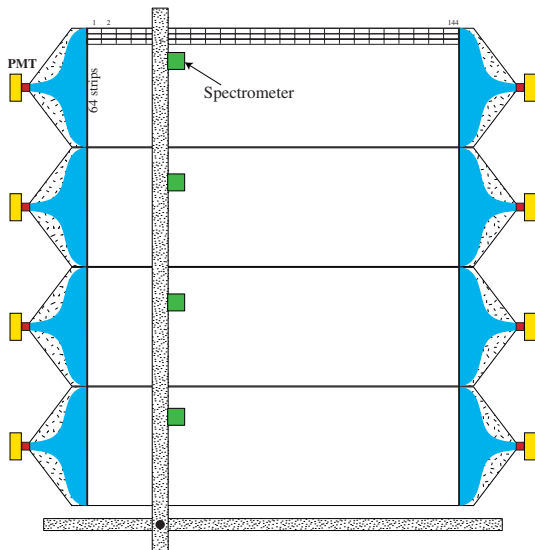

Figure 38. Number of p.e versus the DCS piece position (one point per piece).

Figure 37. Domino Calibration System (DCS).
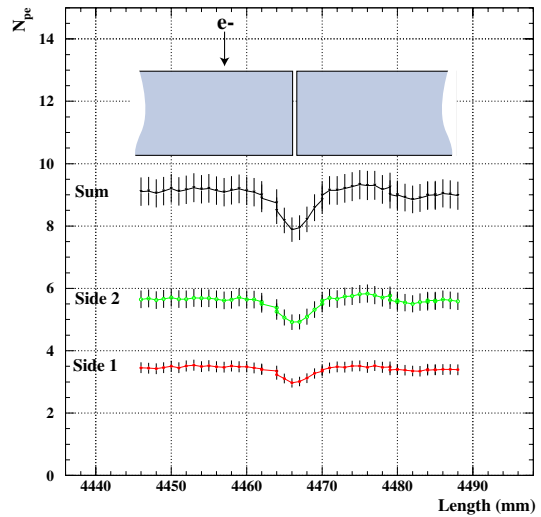
Figure 39. Number of p.e collected by two DCS pieces versus the spectrometer position.

placed vertically somewhere near the OPERA detector. In front of each well numbered scintillator piece a hole on the aluminium sheet could allow their irradiation using a radioactive source (Fig. 37) or, even better, an electron spectrometer equipped with a trigger. An $x - y$ displacement can be used to irradiate all the scintillator strip pieces. For a rate of 50 Hz, 10000 triggers and 30 s displacement per hole, 100 scanning days are needed to irradiate all the pieces using one spectrometer. In case where 4 spectrometers are used (one per module)
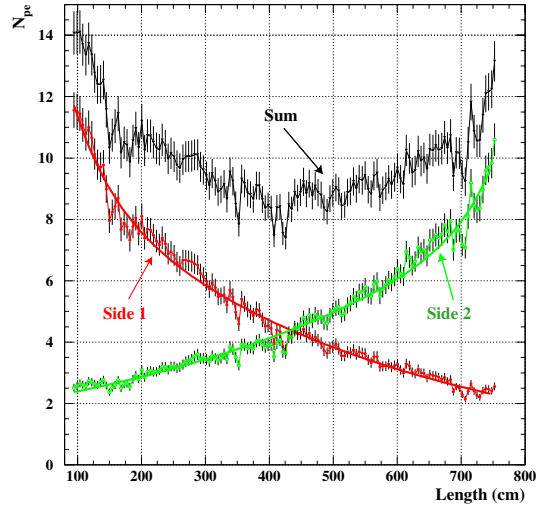
25 days are enough.

Thus, if the module construction is shared by 4 institutes, at the end, each institute will also built one extra module, the DCS one, and one spectrometer with which they will scan their DCS module to obtain the initial calibration point before they send it to Gran Sasso.

If the DCS plane is placed near the veto wall it could also help to the rock muon rejection.

A prototype strip of 144 pieces of 46 mm length each, has been constructed. All the piece faces have

0.3 mm deformation

10 mm

26 mm

Figure 40. Cross section of the prototype scintillator strips.
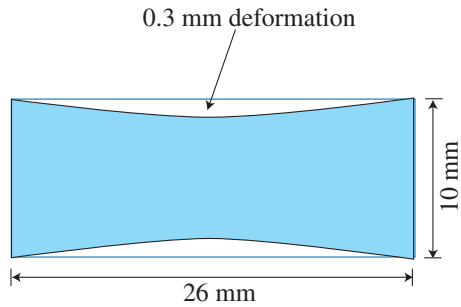

scintillators

fibres

for strip fixing

for cable extraction

for neighbouring module fixing

Figure 42. Zoom on one corner of the end–manifold.

PMT

Cookie

Figure 43. Zoom on cookie region.

been painted with TiO_2. The pieces have been glued together in a metallic guide forming thus a strip of 6.7 m length. The fibre glued on the pieces grooves was a Kuraray Y11 (175) MJ with a diameter of 1.0 mm. Fig. 38 presents the number of p.e detected on each fibre side as a function of the piece position (one point per piece) after a piece irradiation using the electron spectrometer. The number of p.e detected for pieces at 4.3 m (middle of the strip) exceeds 4 and it's at least by 0.5 p.e higher than for normal strips. This is due to the limited light path due to reflections on the lateral faces of each piece. In order to estimate the required positioning accuracy of the spectrometer, a fine scan with a step of 1 mm has been performed between the middle of one piece up to the middle of the next piece (for pieces at a distance of about 5.5 m, see Fig. 38). Fig. 39 presents the obtained result. Between two pieces there is a loss of about 12% but there is a comfortable "plateau" over a distance of 2×15 mm around the middle of each piece. Thus, the spectrometer position accuracy must be less than 1.5 cm, accuracy which can easily be achieved.

6. Prototype

To prove the feasibility of the scintillator modules and learn about their construction, a full scale prototype module has been constructed at Strasbourg using commercial extruded scintillator strips.

6.1. Description

The scintillator strips have been produced by extrusion by Pol.Hi.Tech. The extrusion was done in normal atmosphere without any oxygen or humidity control using a temporary extrusion tool. A calibrator has been used to avoid strip torsion. A cross section is shown schematically by Fig. 40. A deformation has been observed on the strip thickness of a maximum of 0.3 mm at the middle of the strips. This deformation was varying from one strip to the other. Very often the deformation was on both sides and some times on only one side. This
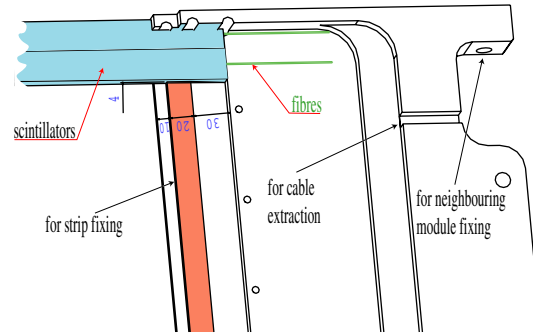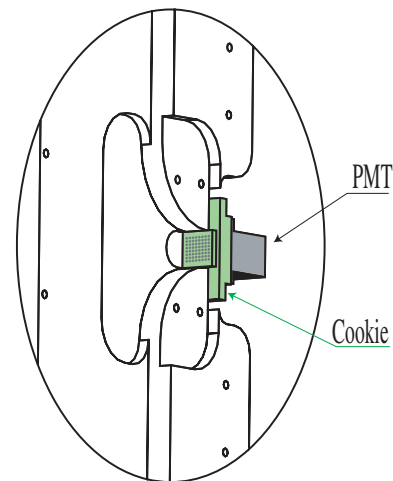
deformation was mainly due to the use of a temporary extrusion tool.

The two end–manifolds, made in Strasbourg, have been produced in a way to take into account all the experimental requirements and conditions (width, rigidity, cable extraction, see section 2). Fig. 41 shows a drawing of the prototype with the two end–manifolds and the aluminium sheets on which the scintillator strips are glued. These aluminium sheets, 0.5 mm thick, assure also a light tightness and protect the scintillator strips. Fig 42 presents more details of the end–manifold where one can see how the strips are fixed on the end–manifolds. Fig. 43, 44 and 45 show more technical details.

The chosen WLS fibres for the prototype were the Kuraray Y11 (175) MJ fibres. For fibre comparison concerning the number of p.e, 48 fibres with a diameter of 1 mm and 16 fibres with a diameter of 1.2 mm have been installed.
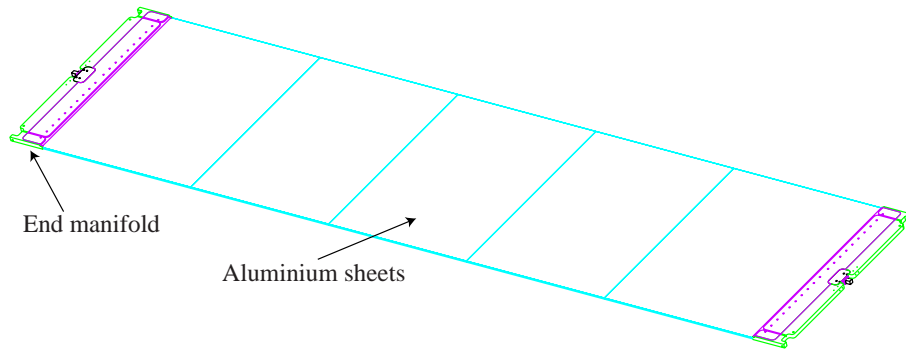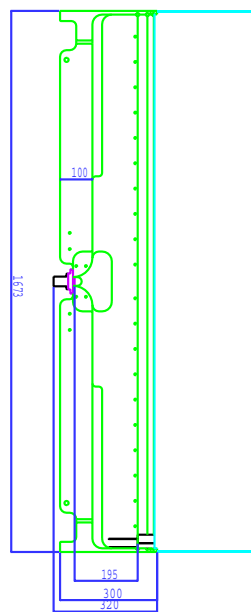
Figure 41. Drawing of the prototype.

Figure 44. Drawing of the end–manifold of the prototype.

Figure 45. Closed end–manifold.
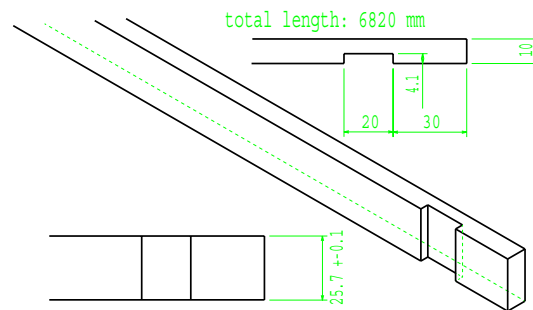
Figure 46. Drawing of one scintillator strip.

6.2. Construction

First of all, the delivered scintillator strips 7 m long have been cut at the right length of 6.82 m. A transversal groove as shown by Fig. 46 has also been machined for strip fixing on the end–manifolds.

The fibre grooves, 1.6 mm depth, have been performed using a 1.6 mm thickness saw and a second one (for comparison) of 1.3 mm thickness. Kuraray Y11 (175) MJ fibres have been glued on the grooves using BC600 glue. In order to keep the fibres at the bottom of the grooves, the fibres have been stretched, while a slide circular shape has been given to the scintillator strips. Nevertheless, some fibres in specific positions near the strip edges went up at the surface and even higher of the scintillator strips during the glue polymerisation. This has induced a more than 20% light loss. In the future, a fibre gluing machine has to be developed.

After the fibres have been glued, the strips have been painted using TiO_2 paint. Three layers have been applied with a total thickness of about 0.15 mm.

In order to glue together the scintillator strips and construct the scintillator module, a rotating table has

Figure 47. Rotating table.

been used as shown by Fig. 47. First, the two end–manifolds have been fixed and aligned on this table at horizontal position. The one side aluminium sheets, 0.5 mm thickness, have also been installed. After that, the scintillator strips have been glued one by one using EPOTEK 310 glue while the ta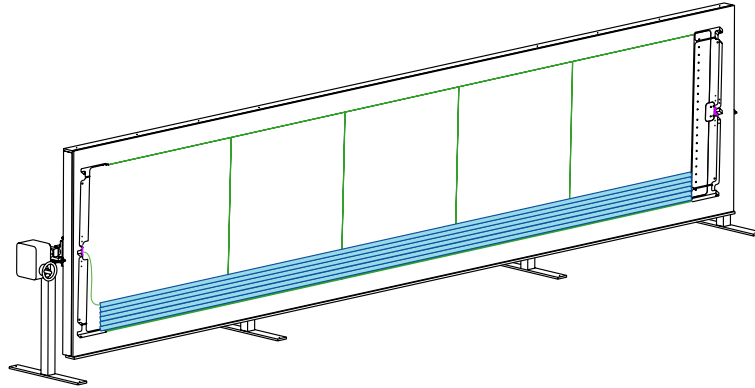ble was in vertical position. A the same time, the fibres were passed inside the 64 holes of each cookie. For a well strip gluing on the aluminium sheets the table has been put in horizontal position and iron bricks have been applied on them.

BC600 glue doped with carbon has been put in the cookie reservoir (Fig. 48) to glue the fibres. Glue has also been applied in the outside part of the cookie in order to bundle the fibres and polish them all together.

At the end, the two Hamamatsu multianode PMT's have been aligned and installed on the fibre cookies produced by University of Bern.

The "upside" aluminium sheets have not been glued in order to be able to perform measurements with the electron spectrometer without loosing extra energy on these sheets.

Figure 48. Monitoring system.

6.3. Monitoring system

A monitoring system produced by U.L. Brussels has been installed in each end–manifold in order to easily test and monitor all the channels (Fig.48). 8 PMMA slides have been inserted between the 8 fibre rows near the cookie. These slides leaves the light (sent by a light injector) escape by only a 1 mm band irradiating thus 8 fibres each. For the light injection a pulsed LED and a light distributor were used.

To study the single electron detection, the PMT characteristics and the fibres in situ, the monitoring system of one side has been used detecting the light on the other side. The light intensity was reduced at the single p.e level. Fig. 49 shows the charge distribution observed on one channel. On this channel 0.034 p.e
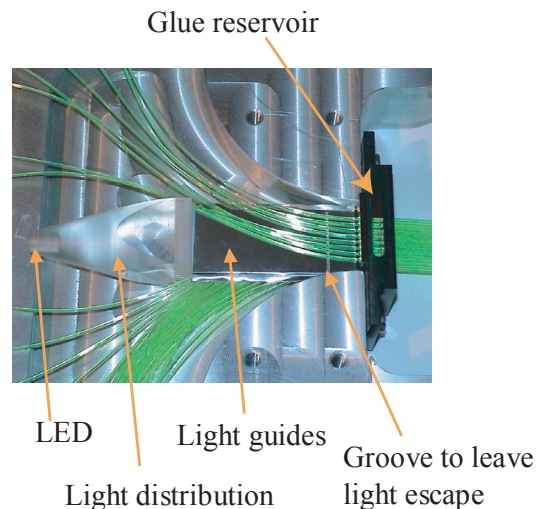
are detected per trigger. Fig. 50 presents the gain, gain dispersion and number of p.e per trigger observed on the one side 64 PMT channels (PMT H.V.=925 V). The non flat distribution of the number of p.e is due to light leaks at the level of the light distributor removed after that.

In the experiment, the gain (Q_1) and dispersion (σ_1) distributions of Fig. 50 will be used for PMT monitoring while the number of p.e (N_{pe}) will be used for both, PMT and fibre ageing monitoring. To disentangle the two effects, the LED on the other end can be used. In this case the fibre ageing does not influence the result because the light path inside the fibre is less than 2 cm (Fig. 48).
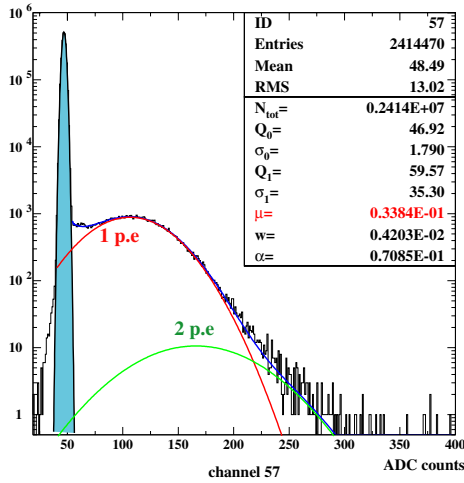
ID	57
Entries	2414470
Mean	48.49
RMS	13.02
$N_{tot}=$	0.2414E+07
$Q_0=$	46.92
$\sigma_0=$	1.790
$Q_1=$	59.57
$\sigma_1=$	35.30
$\mu=$	0.3384E-01
$w=$	0.4203E-02
$\alpha=$	0.7085E-01

Figure 49. Charge distribution for channel 57.

6.4. Measurements

For the different measurements the prototype has been moved on an other table equipped with an $x - y$ displacement remotely controlled where a new electron
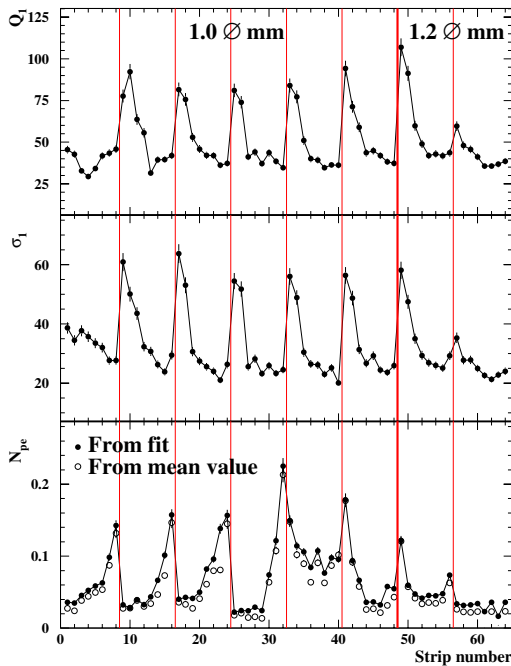

Figure 50. Gain (Q_1), dispersion (σ_1) and number of p.e (N_{pe}) using the monitoring system.

spectrometer (especially developed for this purpose) was fixed. The size and thus the weight of this spectrometer have been considerably reduced compared to the "old" one in order the $x - y$ system to easily carry it without vibrations. In this way, a scanning of all the strips and at any distance can be done.

For all the following measurements preamplifiers produced by Bern have been used.

The main measurement was the number of p.e at the worst position, i.e, at the middle of the scintillator strips and at a distance of 3.41 m from the strip edges. The total fibre length through which the light is propagated varies from 3.8 m to 4.5 m according to the position of the strip inside the module. Fig. 51 shows the number of p.e observed on all channels using the new spectrometer 1.8 MeV electrons. The PMT high voltage was 925 V. Two "holes" have been observed due to a local strip pollution during the fibre groove production. Fibre 63 has been bent too much in the end–manifold. Fig. 52 presents the same distribution but for a distance of 15 cm from the strip edge. The "holes" seen on the previous distribution are slightly seen on this one due to the fact that expansion of the pollution was not uniform and centered around the middle of the strips. The fluctuations observed between channels include also the number of photoelectrons estimation (non perfect fits) and different thickness of the glue inducing an energy loss fluctuation around the fibre groove (this of course will not be a problem for MIP's).

The measurements have been corrected to take into account the non perfect electron spectrum of the spectrometer. Fig. 53 compares the spectra of the "old" and new spectrometers. The 1.8 MeV position is indicated by the maximum of the gaussian part of the well calibrated "old" spectrometer. The applied correction is proportional to the difference between the whole distribution mean value and the gaussian maximum. A certain number of fake triggers due to outside light triggering the trigger PMT's has also been observed and taken into account. It has to be noted that the correction factor 1.17 for the "old" spectrometer was already estimated during the CERN beam test measurements (see section 3.3). This correction factor is 1.33 for the new spectrometer including fake triggers. To remove these triggers a small wire chamber with a drift gap of 3 mm will be installed at the spectrometer exit after the 2 PMT's trigger.

A very important parameter is the cross talk between the scintillator strips. To measure this parameter, the scintillator strip 23 has been scanned with the electron spectrometer at a distance of 15 cm from the strip edge. Fig. 54 shows the charge collected by this strip and the neighbouring strips. When the spectrometer is positioned at the middle of strip 23 a negligible amount of light is observed on neighbouring strips while when the spectrometer is placed near the strip border the light
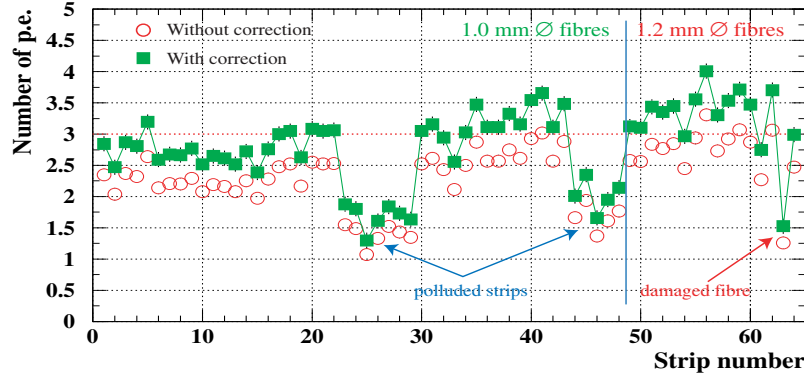
Figure 51. Number of p.e at the middle of the strips versus the strip number.
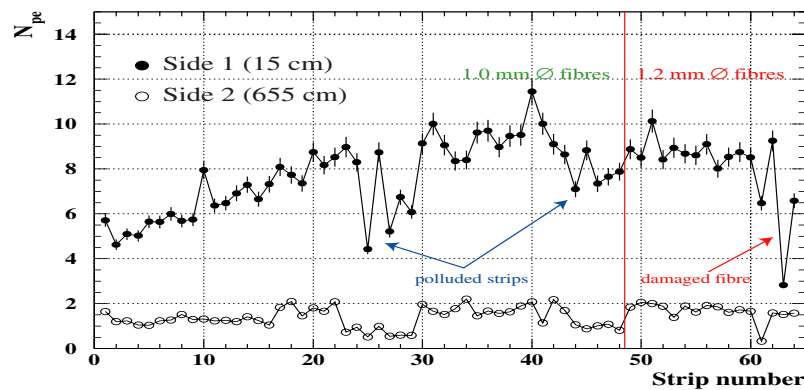

Figure 52. Number of p.e at a distance of 15 cm and 655 cm (opposite side) from the strips edge versus the strip number.

collection by strips 22 and 24 increases significantly. This is due to spectrometer electrons escaping strip 23 (see Fig. 22) and entering in neighbouring strips, which of course, will not be the case for minimum ionising particles. Thus, with three TiO_2 paint layers the strip cross talk is negligible.

6.5. MIP detection efficiency

Although the PMT gain uniformity varies from 1 to 3 between channels (Fig. 50), the MIP detection efficiency is very uniform due to the PMT high gain and low noise allowing a very low threshold (0.3 p.e). Fig. 55 presents the same distribution observed on the same channel than Fig. 49, but this time obtained using the spectrometer at the middle of the strips. A mean value of 3 p.e has been observed. Fig. 56 presents the detection inefficiency of this channel versus the threshold expressed in number of p.e. The MIP detection efficiency is of the order of 99.3% obtained by an "OR" of the signals observed on both sides of the strip. Fig. 57 presents the strip detection efficiency of all the strips for a threshold

of 0.3 p.e (for the corresponding number of p.e see Fig. 51). The same measurement will be repeated using cosmic rays and a threshold applied on the height (voltage) of the signals and not on charge.

7. Electronics

The front-end chip and ADC's can be installed on a board plugged just behind the PMT in order to avoid analogue signal transmission and keep a good measurement quality [1, 5]. The integrated to the detector front–end electronics and their reduced size induce also better EMC (Electro Magnetic Compatibility). On the other hand, extra operations on this board have to be avoided due to the limited access which would make the system debugging and repairing operations difficult. Cooling of electronics has also to be avoided.

A first front–end chip dedicated to the Hamamatsu multianode PMT has been designed and realized by Orsay and Strasbourg. On this version, after a first
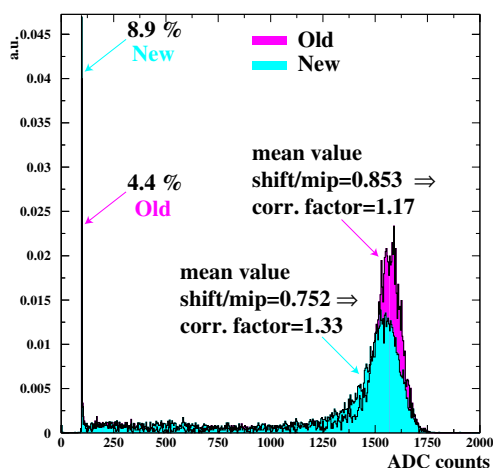
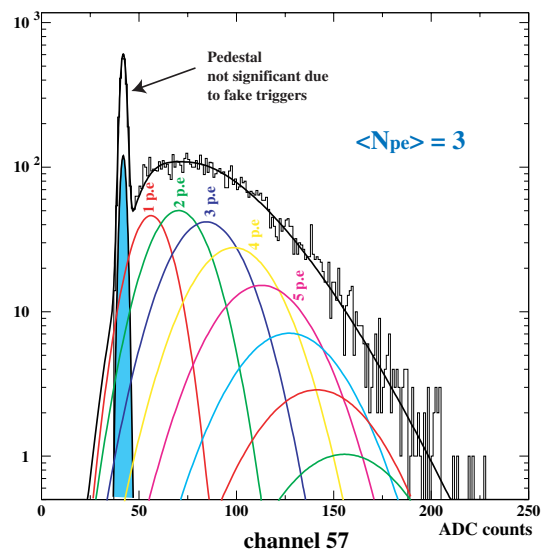**Figure 53.** Spectrum comparison between "old" and new spectrometer.

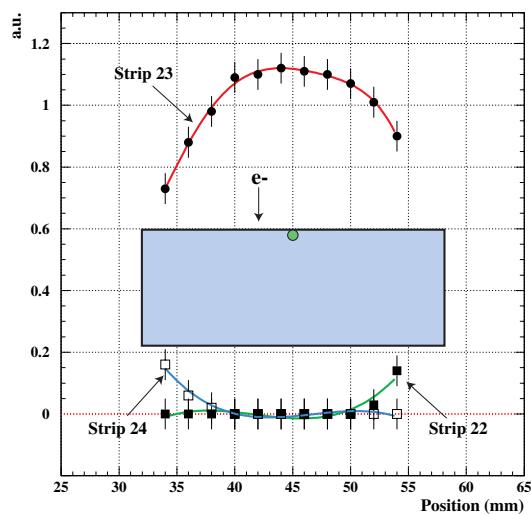**Figure 55.** Charge distribution on channel 57 for electrons entering by the middle of the strip.

Figure 54. Charge collection on irradiated scintillator strip 23 and on neighbouring strips.

8. Noise

The noise affecting plastic scintillator target tracker is expected to come from natural radioactivity, photocathode thermoemission and electronic noise.

A counting rate induced by natural radioactivity of less than 10 Hz per electronic channel is expected. Due to the fact that natural radioactivity will rarely cross the
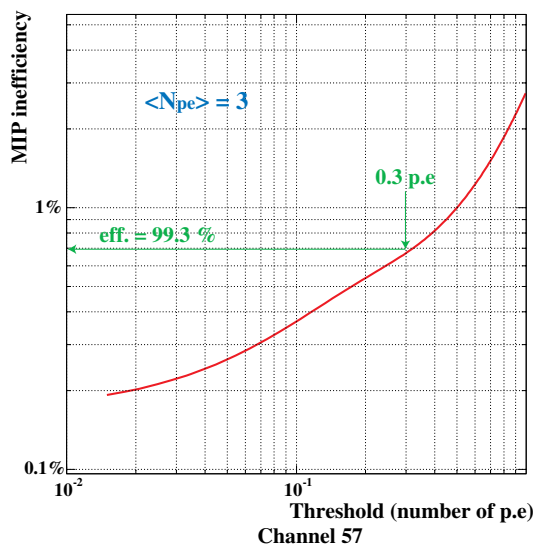
Figure 56. Track detection inefficiency of channel 57 versus threshold for tracks passing by the middle of the strip.

signal preamplification, the signal is split into two ways, a fast one for triggering and a slow one for charge measurement. The gain of the preamplification stage is variable in order to be able to compensate gain variation between PMT channels. Very promising results have already been obtained.
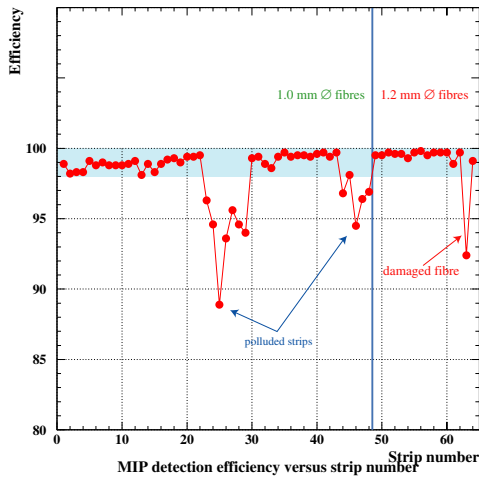
Figure 57. Track detection efficiency for particles passing by the middle of the strips.

two scintillator planes (x and y), after $x - y$ scintillator strip correlation the radioactivity effect is expected to be removed.

On top of radioactivity, the detector and electronic noise has to be added. As already mentioned, a noise less than 10 Hz coming from photocathode thermoemission has been measured on the Hamamatsu PMT with a threshold corresponding to $1/3$ photoelectron. After the first tests on the front–end chip, the electronic noise is expected to be very low. These last two kinds of noise will also be considerably reduced after $x - y$ strip correlation.

9. Long–term stability

The glues used for the prototype construction are already well known and have been used by NEMO experiment. Several glue samples have been followed for more than 7 years.

For scintillator strip ageing, according to MINOS tests, a 10% light decrease is expected over 10 years which is acceptable for our application.

Kuraray fibres are already widely used or tested by high energy experiments in more severe conditions than the OPERA ones (ATLAS) and no ageing effects have been reported.

No ageing is expected for multianode PMT's.

10. Reliability

The target tracker must be extremely reliable due to its non accessibility. In case of problems on a certain

surface of the tracker, the brick finding efficiency of not only the bricks just in front of this dead surface but on several walls upstream will severely be affected. This kind of problems would also induce efficiency evaluation and simulation problems.

The here proposed detector is very reliable due to the robustness of the elements used (plastic scintillator strips, optical fibres, PMT's). Delicate elements, like electronics and PMT's are placed in accessible places. Up to now, on the 7 multianode PMT's bought by the different institutes of the collaboration no spark or any other problem has been observed. Many other tubes have also been tested by MINOS.

11. Installation schedule

The installation schedule of the baseline option is already well defined by the collaboration and for this we refer to the OPERA Implementation Plan.

12. Construction cost

The construction cost of the baseline has already been estimated in the proposal and the Implementation Plan.

13. Running cost

The running cost of plastic scintillators, calibration and monitoring systems is only limited to electrical power consumption which is negligible compared to the spectrometer power consumption. The absence of flammable gases, liquids and very high voltages induces a very light detector survey which could even be done remotely.

14. Forces to built the detector

According to the Implementation Plan, 5 institutes (Bern, Brussels, CERN, Lyon, Strasbourg) are interested to participate to the construction of the target tracker as defined in the Proposal. The same institutes would be involved in the target tracker installation in Gran Sasso.

15. Conclusion

The baseline option defined in the OPERA proposal for the target tracker is a very robust and reliable choice. The construction of the plastic scintillator target tracker prototype has proven the feasibility of the technic and allowed a better tune of the different parameters. The number of photoelectrons in the most difficult case obtained on the prototype (~ 3) is already satisfactory. It can only be improved and has room for improvement using co–extrusion of plastic scintillators under neutral

atmosphere. Monitoring and calibration systems are also tested and proposed for testing, debugging and ageing following of the detector.

References

[1] OPERA proposal, *"An appearance experiment to search for $\nu_\mu \leftrightarrow \nu_\tau$ oscillations in the CNGS beam"*, CERN/SPSC 2000–028, SPSC/P318, LNGS P25/2000, July 10, 2000.

[2] Hamamatsu Photonics K.K., Electron Tube Center, 314–5, Shimokanzo, Toyooka–village, Iwata–gun, Shizuoka–ken, 438–0193, Japan.

[3] E. Ables et al. (MINOS), Fermilab Proposal P-875 (1995).

[4] I216 proposal, CERN–SPSC/99–26, SPSC/P311, August 30, 1999.

[5] A Data Acquisition System for the OPERA Neutrino Long Base Line Experiment, OPERA note 17, June 6, 2000.